Supporting Information

Table of Contents

Sample characteristics

Table S1. Designations and sample characteristics.[1]

Sample designation	FHI-database ID	Synthesis yield (%)	K/Ir (10^{-3})	Cl/Ir (10^{-3})	S_{BET} ($m^2\ g^{-1}$)	Physisorbed H_2O (wt.%)	H_2O removed via dehydroxylation (wt.%)	$IrO_x(OH)_y$		Ir^0-content (mol.%)	Avg. Ir-oxidation state (oxidic phase)
								x	y		
MW_1	21009	51	2.5	433	217	2.7	6.0	0.56	1.68	6.0	0.56
MW_4	21404	97	3.9	299	165	2.6	7.0	0.54	1.94	7.0	0.54
MW_5	21011	99	18.4	0	104	1.9	6.7	0.86	1.79	6.7	0.86
MW_7	21130	100	91.0	0	56	1.9	3.6	1.17	0.93	3.6	1.17
MW_10	21013	99	112.6	0	175	2.6	2.5	1.21	0.66	2.5	1.21
MW_50	21015	72	92	0	7	1.7	2.3	1.15	0.58	2.3	1.15
MW_100	21017	35	36.4	0	16	1.2	1.05	n.d.	n.d.	1.05	n.d.
SA-IrO_2	21285	-	0	0	4	0.1	0	2	0	0	2
AA-IrO_x	20233	-	0	0	33	0.9	5.1	1.09	1.34	5.1	1.09

Electrochemical testing

The tests were conducted in a standard three-compartment glass cell containing approx. 100mL of H_2SO_4 (0,5 mol.L^{-1}). The reference electrode was a saturated calomel electrode (SCE) at +0,241V vs. standard hydrogen electrode (SHE), the counter-electrode was a platinized wire. The samples were deposited on the anode (rotating disk electrode, RDE, Pine Research Instrumentation) using catalyst inks dried for 30min at 60°C. The inks were prepared by suspending 4mg of sample in 6 mL Milli–Q H_2O and 4 mL isopropanol (Sigma Aldrich), followed by sonication for 30min. Prior to use, the RDE was repeatedly cleaned with Milli–Q water and isopropanol, after mirror-polishing with alumina bead slurries (Buehler, 1 µm and 0,05 µm). Measurements were carried out with a VSP-multichannel potentiostat (Biologic Instruments) and were corrected at 85% for ohmic drop using high-frequency impedance determination of the electrolyte resistance (4 measurements, 100kHz, 20mV amplitude, open circuit potential).

Transmission Electron Microscopy

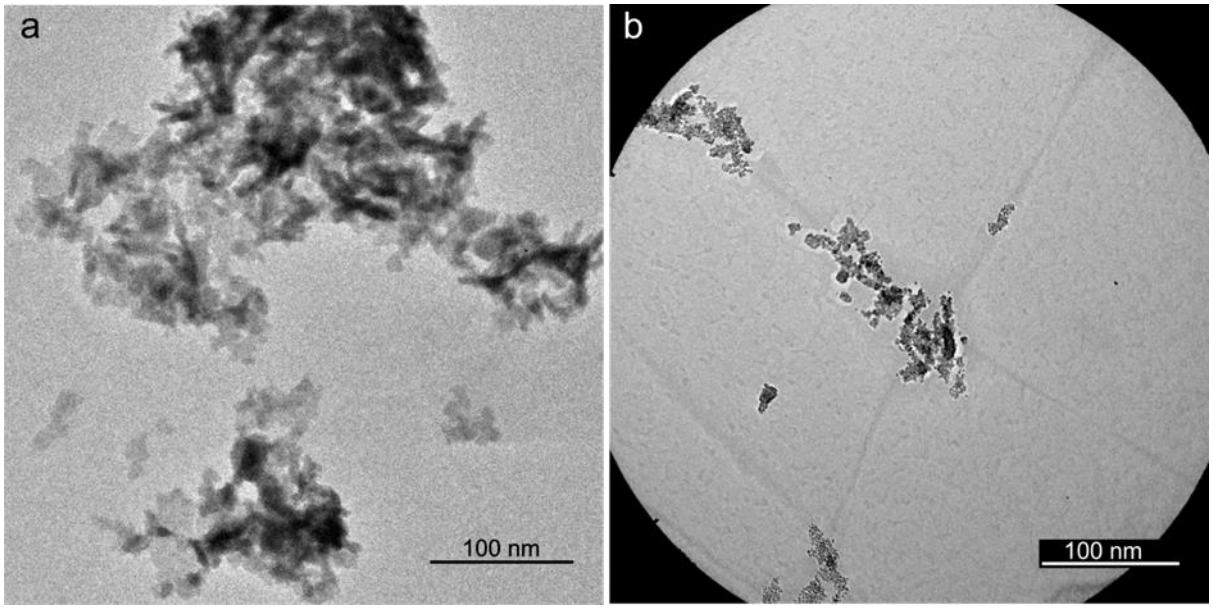

Fig.S1 (a) Image of sample area obtained after SAED pattern (Figure 1a) and (b) sample area before SAED pattern (Figure 1b).

Raman spectroscopy

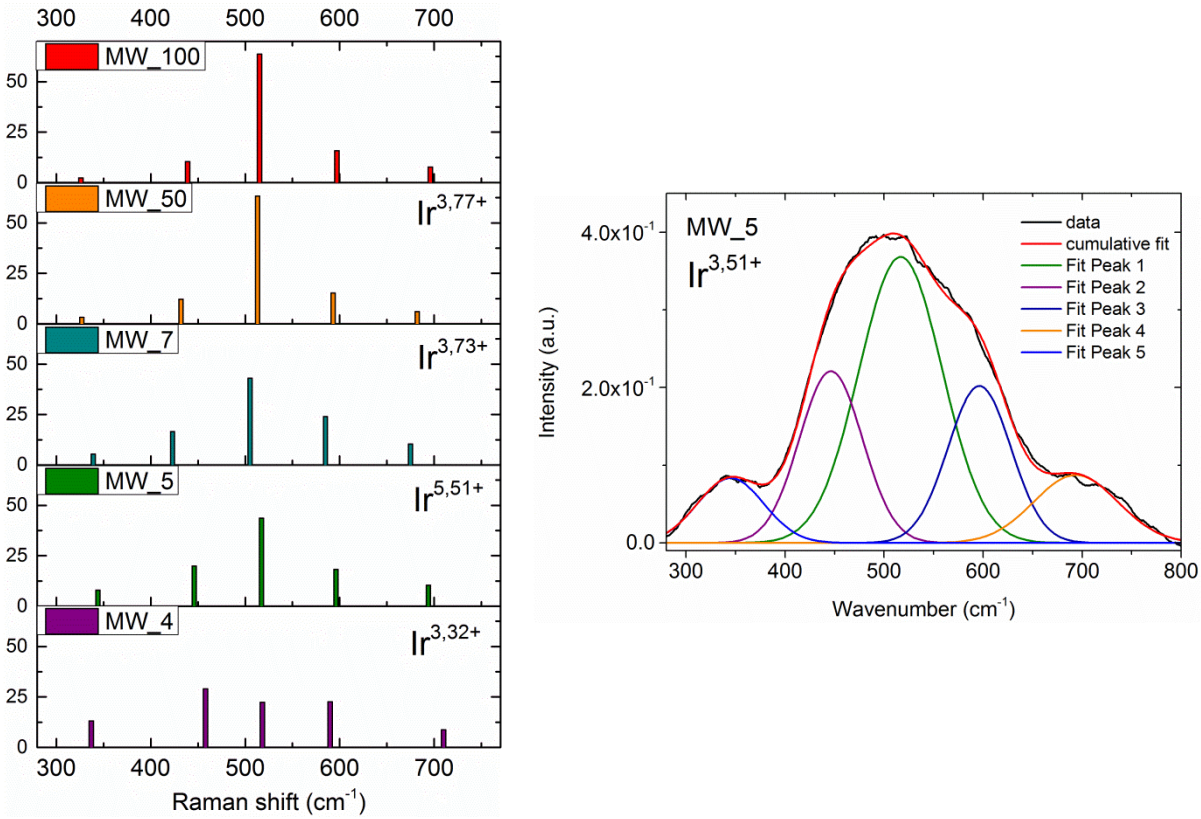

Figure S2. shows the relative peak areas and positions of the five Gaussian peaks used to tentatively fit the Raman data recorded for MW_4, MW_5, MW_7, MW_50 and MW_100 (left). The resulting fit for MW_5 is shown on the right as an example.

Table S2. List of parameters for peaks I-V after fitting.

	Peak I		Peak II		Peak III		Peak IV		Peak V	
Sample	**Center [cm^{-1}]**	**Area [%]**	**Center [cm^{-1}]**	**Area [%]**	**Center [cm^{-1}]**	**Area [%]**	**Center [cm^{-1}]**	**Area [%]**	**Center [cm^{-1}]**	**Area [%]**
MW_4	337	13	458	29	518	22	590	23	710	9
MW_5	344	8	446	20	517	44	596	18	694	10
MW_7	339	5	423	17	505	43	585	24	675	10
MW_50	327	3	432	12	513	63	593	15	682	6
MW_100	326	2	439	10	515	64	597	16	696	8

Calculated dominant Raman modes

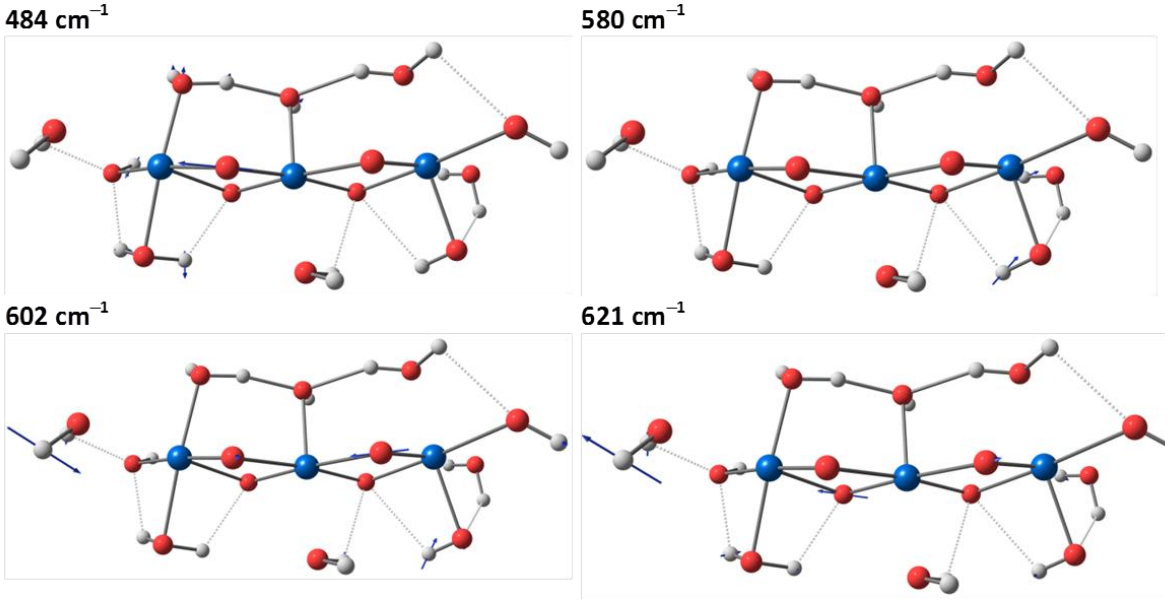

Figure S3. Overview of the normal modes that dominate the calculated Raman spectrum of the Ir^{IV} Ir^{IV} Ir^{IV} trimer. The lower frequency is dominated by a μ-oxo vibration, the larger 3 by hydroxo vibrations.

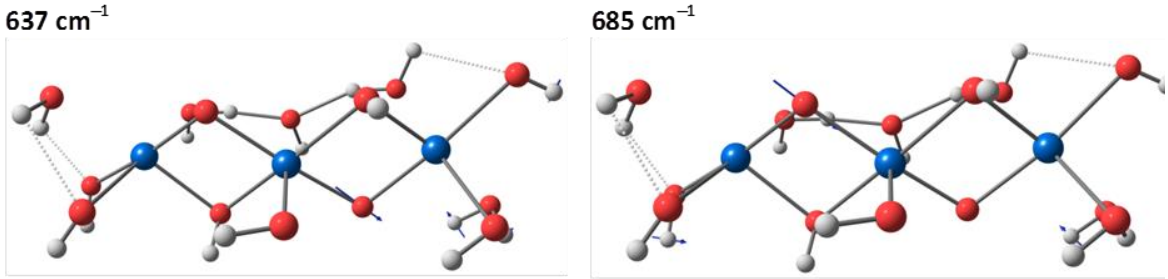

Figure S4. Overview of the normal modes that dominate the calculated Raman spectrum of the singly reduced trimer $Ir^{IV}Ir^{III}Ir^{IV}$. The spectrum is dominated by μ-oxo vibrations. These vibrations are more localized than the ones of the oxidized trimer and therefore shifted to higher frequencies as compared to those of the oxidized trimer.

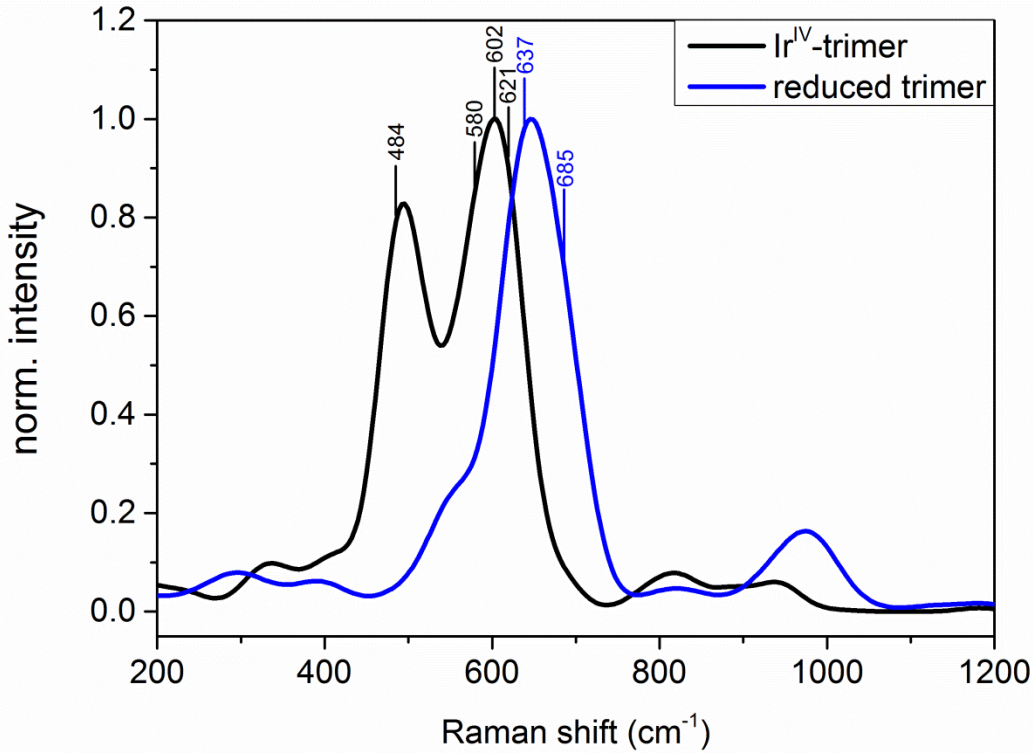

Figure S5. Calculated Raman spectra of the IR-trimer in its oxidized and reduced form. The main Raman-active modes shown in Fig. S3 and Fig. S4 are indicated.

Note that it is quite clear that a Raman calculation on a well-defined structure as a model for an amorphous material has intrinsic limitations. For this reason, we prefer to define regions in the experimental spectrum (cf. Figure 3). The calculated Raman spectrum reproduces the structure observed in the experimental spectrum, but certainly should not be over-interpreted by the comparing peak positions to the wavenumber with those in experiment.

Cartesian coordinates (Å) of geometry-optimized clusters

Ir^{IV} Ir^{IV} Ir^{IV} trimer model

O	-0.56662317939086	-0.42446133106470	-1.18044659219642
O	0.53933184468527	-0.32091685050492	1.00858281161036
O	2.30366298946447	-1.20586656560217	-0.69779842648356
O	-1.90599078260942	1.07598119453924	0.91166810754166
H	-1.53097301277179	-3.25489224375562	-0.09012289084337
H	1.92511596734510	-1.58878237440869	0.12575551261695
H	0.37717843934692	2.85311584618865	0.00133458101118
O	-0.77787927880585	-2.89689546543435	0.41371405575550
O	-0.10271796498406	2.18041950238608	-0.49755875677927
Ir	1.07778653529812	0.48152273141922	-0.70634419072276
Ir	-1.32127378436932	-0.83808429047232	0.59907985395111
H	2.63012423392848	1.69933910598993	-2.21599403866367
H	1.95725186419958	0.77363596894144	-3.29793736388329
O	1.77576990687063	1.40962685705603	-2.59574474175234
O	-2.05098852209210	-1.47756452825712	2.37449890043553
H	3.10628003363515	-0.71041313637929	-0.41743820628628
H	-1.68010750492233	1.22072671391972	1.84161607193362
O	2.90942460831755	1.30254759112380	-0.29322932051304
H	3.01488454542175	1.63303307988711	0.60375751674304
O	-3.10383513476772	-1.45566127115077	0.13237576638231
Ir	-3.90938410216041	-1.75075274082773	1.86917582325691
O	-5.74333056890572	-1.93462786806336	1.18503042016313

H	-6.23570125876549	-2.65244138509053	1.59938424858513
H	-0.89970338288247	1.85920949526814	0.07627493280330
O	-4.66600467710594	-2.12644053775424	3.90803398088771
H	-4.02888817976186	-1.74686239818963	4.52869086722102
H	-4.41244509268387	-3.07379634445428	3.78456549040318
O	-3.59967244747833	-3.69695772713004	2.19939728334663
H	-2.69871378717513	-3.75073478612836	2.54795966643378
O	-4.40261804852076	0.34016785140485	1.62806747334439
H	-3.64041585653329	0.74837083160021	1.14531758131545
H	-5.15812735157836	0.26970772556010	1.02313659966838
H	-0.95813193924798	-3.14481352761636	1.34034080971374

Reduced $Ir^{IV}Ir^{III}Ir^{IV}$ trimer model

O	-0.570358	-0.422373	-1.026096
O	0.553681	-0.162797	1.214576
O	2.213967	-1.126480	-1.059332
O	-2.040979	1.005309	0.872191
H	-2.910224	-2.616053	-0.273926
H	1.131855	-0.908140	1.424803
H	0.405780	2.727704	0.405782
O	-0.586269	-2.823721	0.441029
O	-0.087555	2.237194	-0.263131
Ir	1.120110	0.510986	-0.646806
Ir	-1.263207	-0.979007	0.638369
H	2.594117	1.521561	-2.117675
H	2.180908	0.156926	-2.744553
O	1.836814	1.056620	-2.566728
O	-2.077383	-1.308238	2.336025
H	3.092470	-0.976206	-0.688142
H	-1.900655	1.139817	1.818600
O	2.808653	1.688333	-0.347020
H	3.426859	1.323224	0.292213
O	-3.095166	-1.716098	0.031979
Ir	-3.935651	-1.811137	1.886967
O	-5.809904	-2.167954	1.197620
H	-6.406221	-2.326899	1.937300
H	-0.930796	1.850058	0.179269
O	-4.501778	-2.058726	3.939077
H	-3.808682	-1.566933	4.402106
H	-4.116716	-2.987900	3.779730
O	-3.538665	-3.716037	2.407640
H	-2.580466	-3.818070	2.337273
O	-4.474593	0.204210	1.387744
H	-3.643314	0.618261	0.994561
H	-5.120415	0.007383	0.691141
H	0.257066	-2.758378	-0.027444

Photoemission spectroscopy

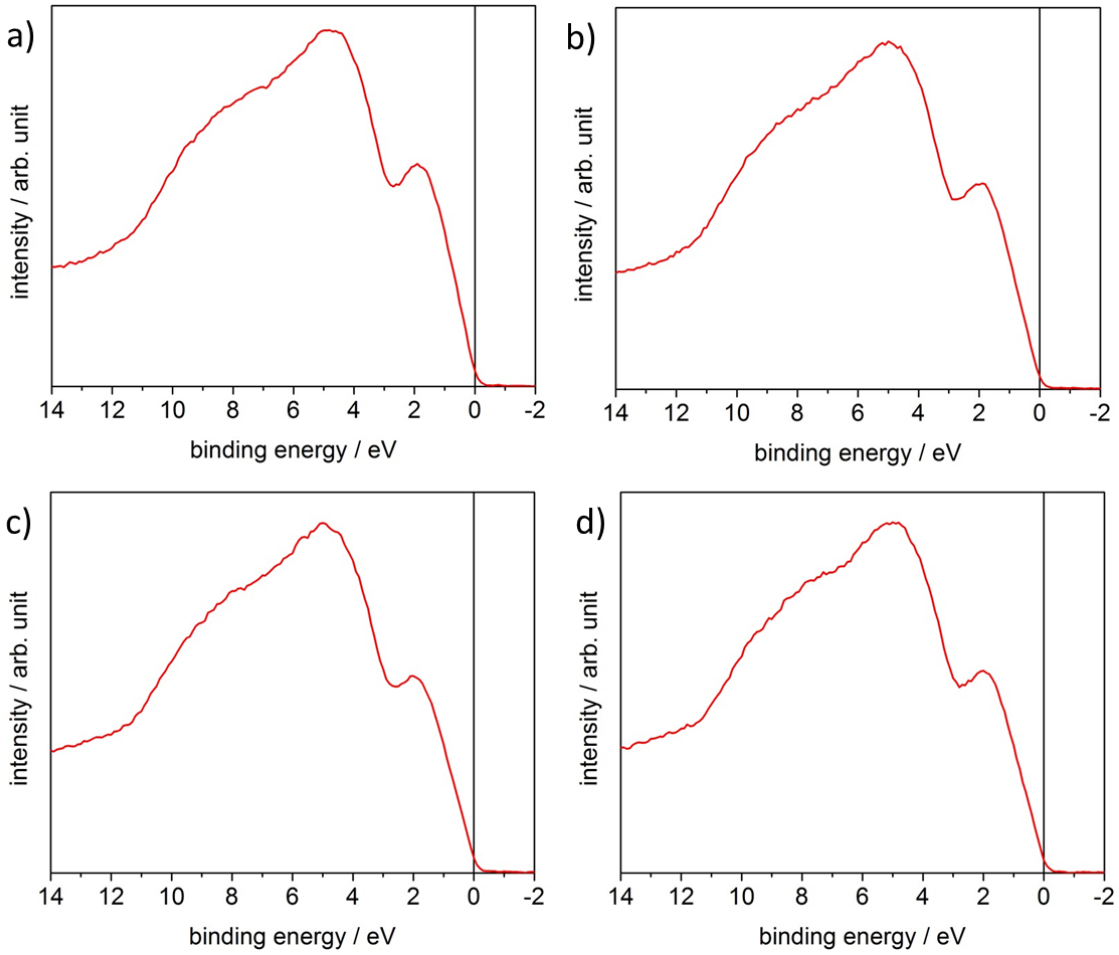

Figure S6. XPS-spectra of MW-prepared Ir-oxohydroxides in the valence band-region at excitation energies of 450 eV for (a)MW_5, (b) MW_10, (c) MW_50 and (d) MW_100.

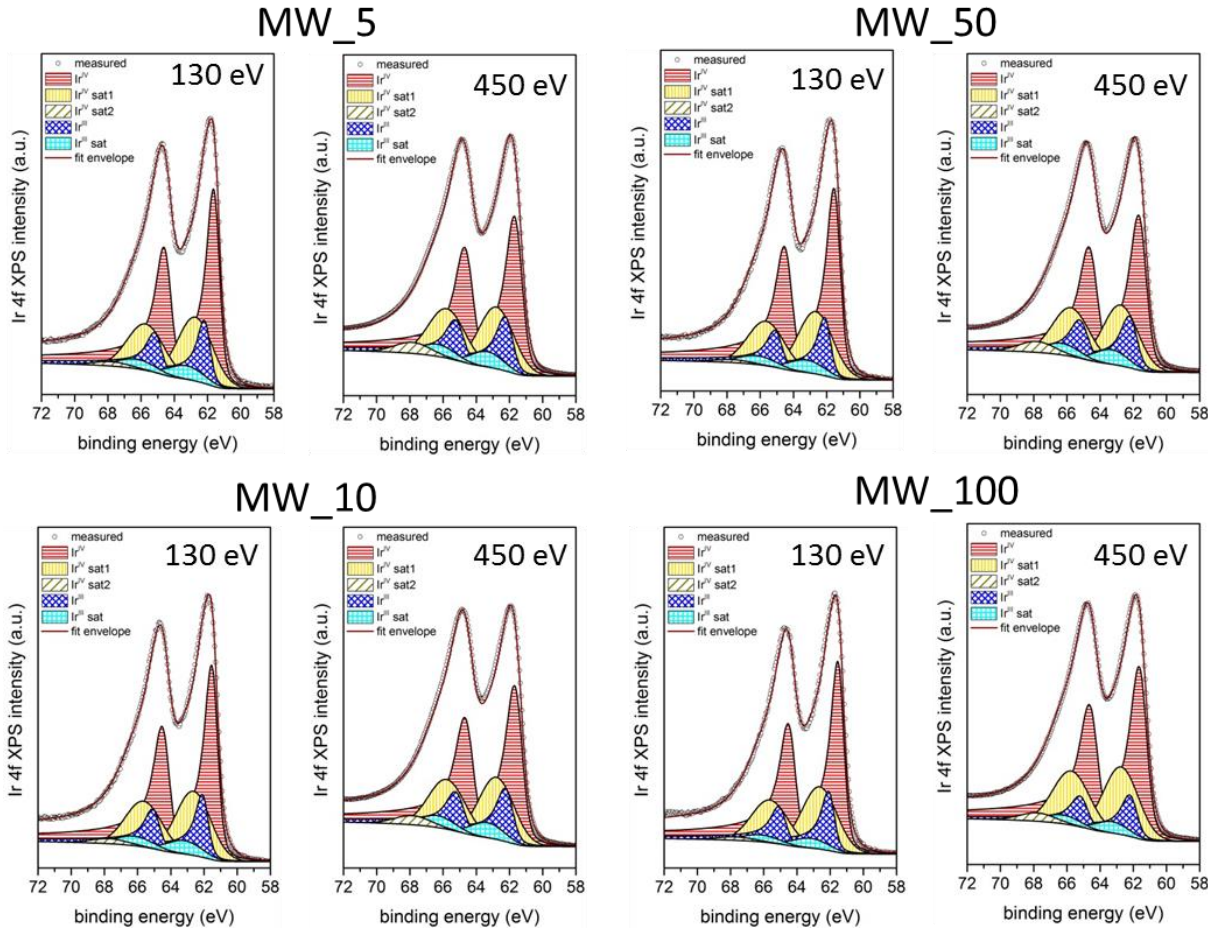

Figure S7. XPS-spectra of the MW-prepared Ir-oxohydroxides in the Ir 4f-region at kinetic energies of 130 and 450 eV.

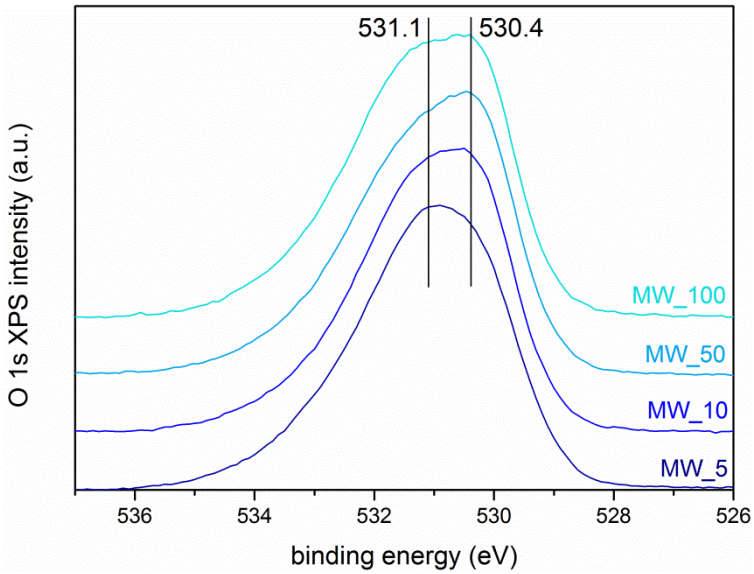

Figure S8. XPS-spectra of MW-prepared Ir-oxohydroxides in the O 1s-region at excitation energies of 450 eV

RT- CO-oxidation

The reactor setup was equipped with an on-line gas analyzer (X-Stream, Emerson/Rosemount) to quantify O_2, CO and CO_2. The temperature in the catalyst bed could be directly monitored by an analog connection to the gas analyzer. Every gas line was equipped with a mass-flow controller (E1-flow, Bronkhorst). The CO-gas line was equipped with a carbonyl remover, consisting of a tube filled with inert SiC and heated to 573 K as well as a CO_2-trap consisting of a crushed-KOH-filled cartridge. The carrier gas line was equipped with a water and oxygen filter. The reactor itself was a U-tube with an inner diameter of 5 mm, made of glass-lined steel (SGE).

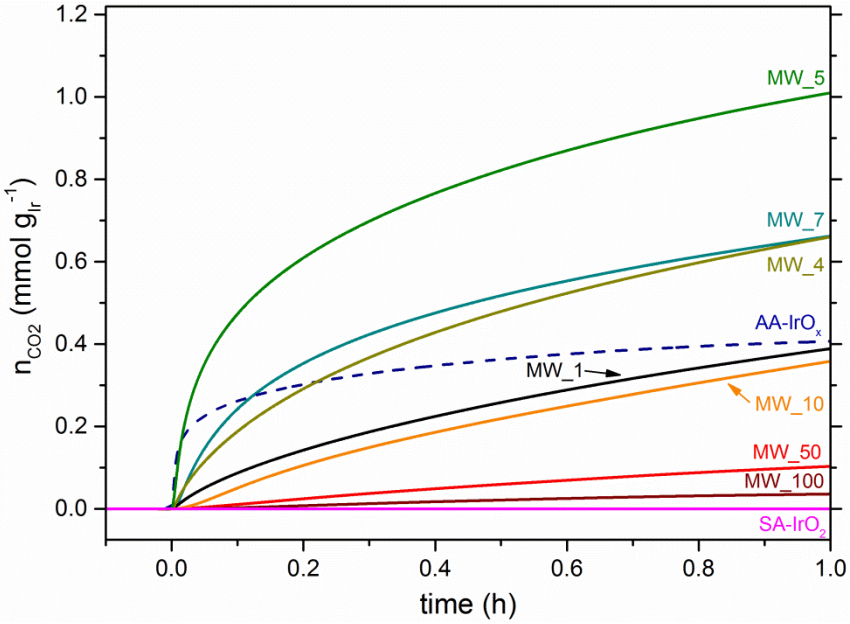

Figure S9. CO_2 evolved during the first switch from 100%-He to 1%-CO/He for the MW-Ir-compounds as well as the reference samples

DRIFTS

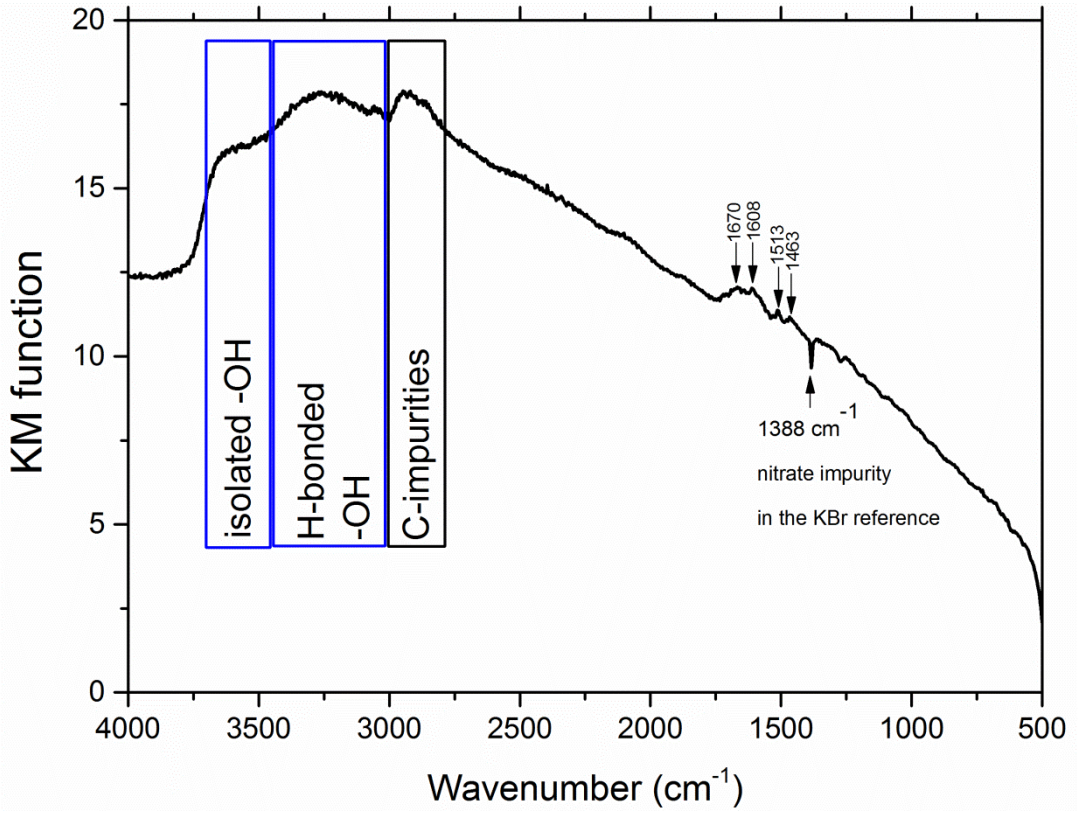

Figure S10. DRIFTS spectra recorded for MW_5 at RT after degassing overnight at 40°C in vacuum.

Small contributions between 1670 and 1450 cm-1 are attributed to the vibrations modes of various carbonate species probably formed during the synthesis from atmospheric CO_2 dissolved in the basic precursor solution.[2]

Low-temperature CO-adsorption

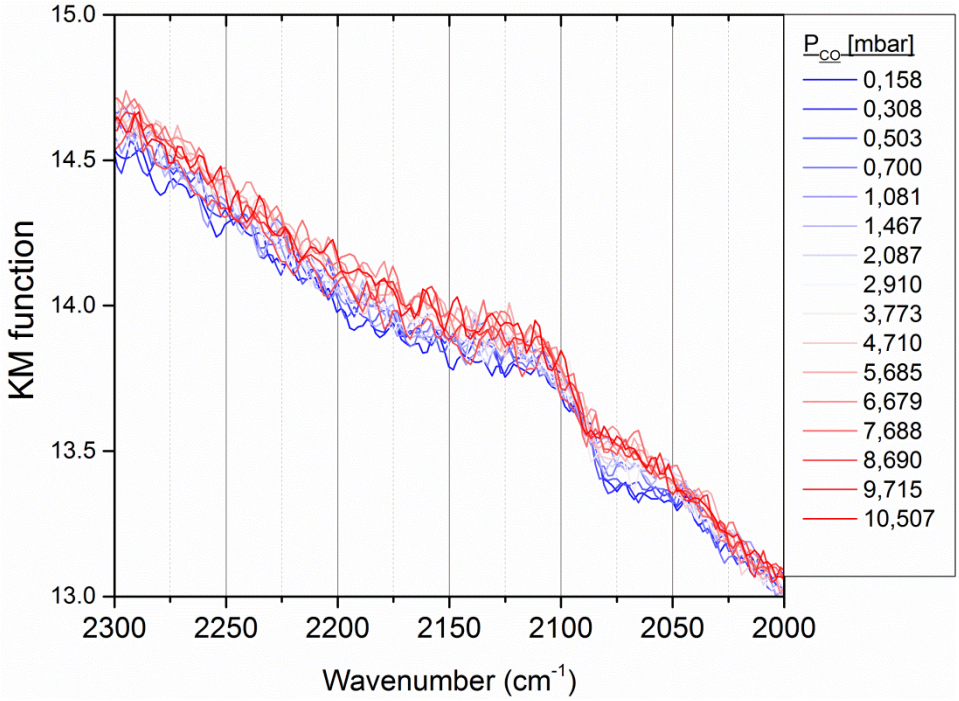

Figure S11. shows the small changes in DRIFTS-spectra of MW_5 upon gradual CO-addition at 77K

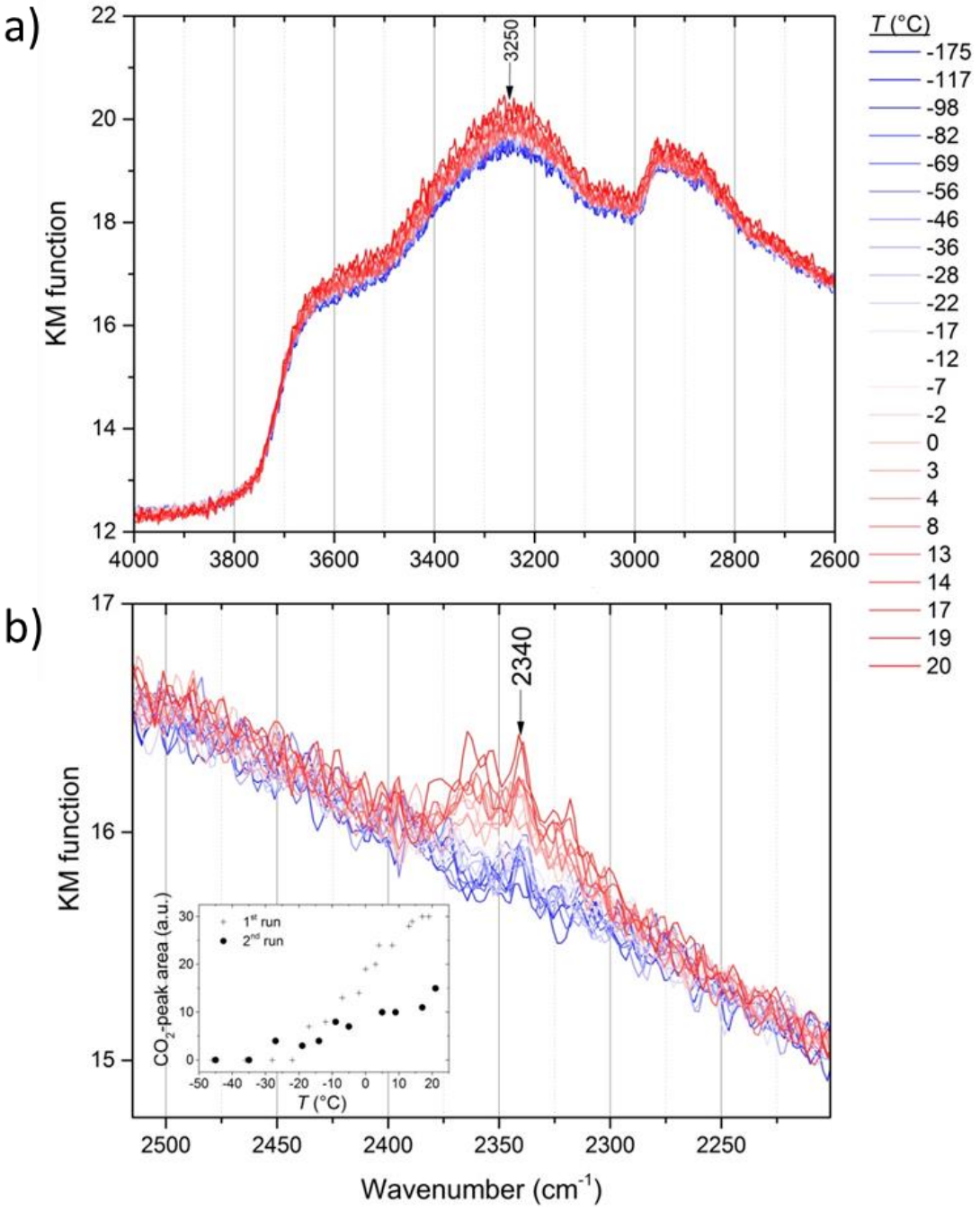

Figure S12. DRIFTS spectra of MW_5 after CO-addition at liquid-nitrogen-temperature during the first warm-up to room-temperature **(a)** in the OH-region and (b) in the CO_2-region. The inset in **(b)** shows the integrated area under the CO_2-related peak as a function of temperature during the first experiment and during its repetition with the same sample.

CO-oxidation of MW_5 in the Raman cell

Approx. 40 mg of sample MW_5 were placed in an air-tight cell designed for on-stream Raman-spectroscopic investigation of powdered catalysts. The Raman spectra are recorded through a quartz window.

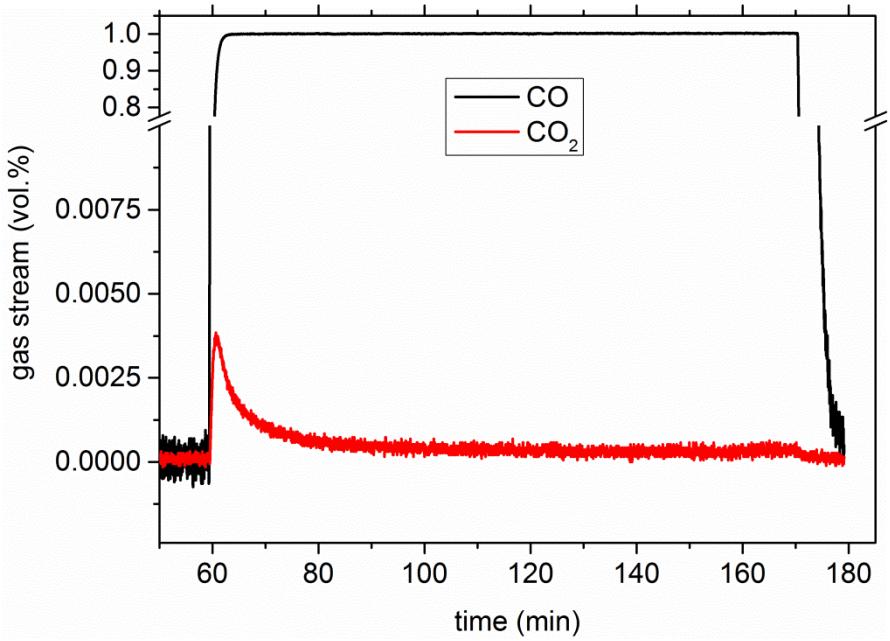

Figure S13. Gas stream signals during the CO-treatment of MW_5 in the Raman cell

Raman spectra before/after CO-oxidation

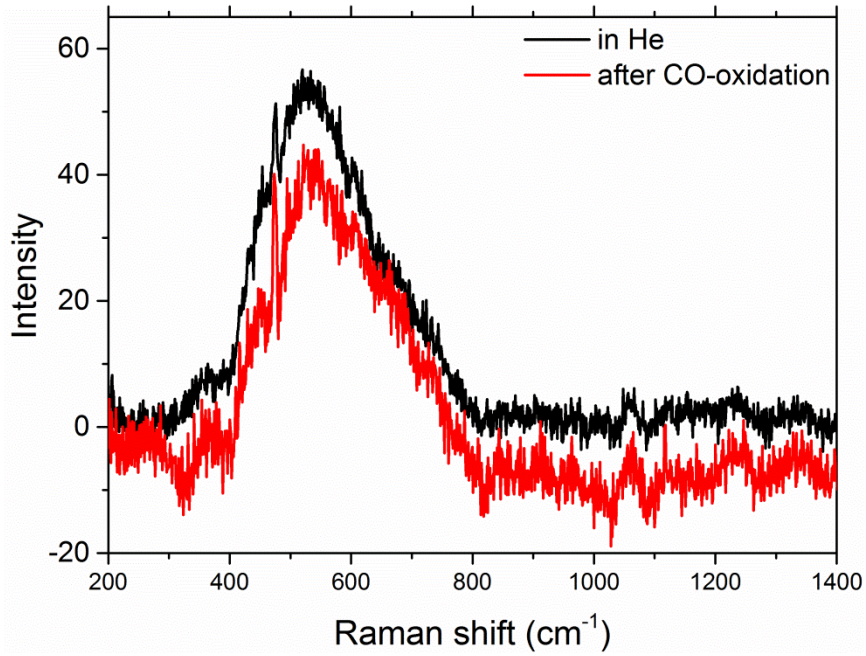

Figure S14. shows the background-substracted Raman spectra of MW_5 recorded before and after CO-treatment at room temperature for 1h in the Raman-cell

References

(1) Massué, C.; Huang, X.; Tarasov, A.; Ranjan, C.; Cap, S.; Schlögl, R. *ChemSusChem* **2017**, *10*, 1958.

(2) Hadjiivanov, K. I.; Vayssilov, G. N. *Adv. Catal.* **2002**, *47*, 307.